



# Multi-Objective Optimization of Aerodynamic Performance for a Small Single-Stage Turbine

Q. Tang, H. Wu<sup>†</sup> and H. Lou

School of Power and Energy, Northwestern Polytechnical University, Xi'an, Shanxi, 710129, China

<sup>†</sup>Corresponding Author E-mail: [wuhu@nwpu.edu.cn](mailto:wuhu@nwpu.edu.cn)

(Received November 15, 2021; accepted May 9, 2022)

## ABSTRACT

In order to improve the performance of single-stage turbines, blade profiling optimization was conducted for the guide vane and rotor under design condition. Support vector regression (SVR) and non-dominated sorting genetic algorithm-II (NSGA-II) were used to execute the optimization, with the objective of maximizing the efficiency and total pressure ratio of single-stage turbines. The gas turbine chosen for the initial study was the KJ66, which is one of the most robust and primitive small gas turbine designs available. The influence mechanism of the stator and rotor profiling on flow field and performance was discussed. The results revealed that compared with the prototype, the adiabatic efficiency increased by 5.95% and the total pressure ratio increased by 0.9%. Furthermore, the matching of flows between the stator blade and rotor blade obviously improved. The optimized guide vane suppressed the flow separation by increasing the leading edge and improving the distribution of the inlet angle of attack. The load distribution of rotors with a 50% spanwise position changed from the original "C" loaded to post-loaded. The leading load obviously decreased, and the angle of attack was smaller than that of the prototype, which effectively weakened the flow separation at the leading edge of the rotor. Compared with the original rotor, the higher lean angle and pressure ratio of the turbine stage also improved. However, the leakage loss near the shroud of the rotor increased, which led to decreased efficiency.

**Keywords:** Turbine; Performance; Blade profiling; Multi-objective optimization; Flow separation.

## NOMENCLATURE

CFD	Computational Fluid Dynamics	SA	Sensitivity Analysis
$k$	turbulence kinetic energy	$s_j p_j$	middle curve of the guide vane
MGT	Micro Gas Turbine	$T_3^*$	total temperature at the inlet
MTE	Micro Turbojet Engines	$T_4^*$	total temperature at the outlet
$m_{ori}$	original mass flow rate	UAV	Unmanned Aerial Vehicles
$p_3^*$	total pressure at the inlet	$\gamma$	specific heat ratio
$p_4^*$	total pressure at the outlet	$\eta$	adiabatic efficiency
RSM	Response Surface Method	$\pi$	pressure ratio
$r_j p_j$	chord middle curve of rotor	$\omega$	specific turbulence dissipation rate
SVR	Support Vector Regression		

## 1. INTRODUCTION

Researches have revealed that micro-turbines are usually presented in units of less than 350 kW, while micro turbojet engines (MTE) are presented in units of less than 1000 N of thrust (Tian 2003). Micro turbojet engines have been widely used in model aircrafts and unmanned aerial vehicles (UAV) due to

its small size, high thrust-to-weight ratio, high energy density, and easy maintenance. Axial turbines are one of the most important components of micro-engines, and its performance has a great impact on the overall performance of the entire micro turbojet engine.

Axial turbine aerodynamic designs have been developed using analytical methods, including

similarity analysis, meanline modelling, and 2D/3D blade design (Moustapha *et al.* 2003). Among these methods, the meanline design approach has become the common method in turbine preliminary sizing, and turbine efficiency can be calculated using one of the published correlations (Ainley and Mathieson 1951; Balje 1968; Smith 1965; Dunham and Came 1970; Kacker and Okapuu 1982). The performance prediction method makes many simplified assumptions. However, the use of traditional approaches (e.g. Soderberg, Ainley and Traupel) in gas turbine design has led to inaccurate results. Therefore, significant improvements are required (Dunham and Came 1970; Craig and Cox 1970). Recently, researchers are attempting to develop loss correlations, in order to maximize the efficiency or total pressure ratio, by varying independent blade geometry parameters for on or off design conditions, and applying the optimization method on turbine design (Moustapha *et al.* 1990; Benner *et al.* 2006a, 2006b, 2004; Zhu and Sjolander 2005; Wakeley and Hey 1997). For instance, Balje (1968) conducted an optimization to simplify the loss prediction correlation integrated with the meanline approach. The optimization was performed through varying blade profile geometry parameters. The results revealed that the turbine efficiency improved by 5%. In another study, Massardo *et al.* (1990) utilized a multi-objective algorithm for the turbine optimization of blade geometry. The results revealed that the turbine efficiency increased by 1.7%.

The progress of computational fluid dynamics (CFD) methods and the power of computers have led to the replacement of a considerable part of the test, with fast and cheap calculations, allowing for the prediction of flow behavior in individual MTE units with reasonable accuracy. Thus, a number of numerical optimization methods have been developed for turbine design optimization. These optimization techniques can also be combined with the CFD solver to achieve a detailed design. For instance, Basson (2014) developed five design-related capabilities, and applied these to the axial-flow turbine design for the existing micro gas turbine engine, BMT 120 KS. The results revealed that the total temperature varied due to the non-uniform distribution of turbine outlet flow temperature. In another study, Moroz *et al.* (2004) provided a detailed process for axial turbine flow path optimization based on the DOE and FEA package. The capability of commercial CFD in turbine optimization through 3D simulation was proven in their study. Similar investigations were conducted by Mohamed and Shaaban (2013) to improve turbine efficiency using an automated optimization algorithm and standard aerofoil geometries, NACA0012 and NACA0021. Citing another example Yang and Xiao (2014) investigated the optimization design of a pump-turbine impeller using CFD and the response surface method (RSM) to select an optimum design point. The comparison of simulation results with the conducted tests clearly revealed that the multi-objective optimization based on CFD and RSM is a good optimization strategy for turbine and pump designs.



(a) Guide Vane



(b) Rotor

**Fig. 1. KJ66 turbine model.**

The axial turbine optimization was validated against experimental and numerical data of the prototype. One well-known study on small axial turbines is the KJ66 (Fig.1), which was carried out by Murray (2009). He experimentally measured the total pressure ratio and efficiency. However, the experimental data for maximum operating speed was poor. Recently (Li, 2019) used the FLoEFD software to calculate the KJ66 turbine performance. The calculation error was small, and the results were in good agreement with the experimental results. To the author's best knowledge, the simultaneous optimization of the guide vane and rotor of the KJ66 turbine has not been implemented in open literature.

This manuscript was organized as follows. In section 2, the optimization details were elucidated exhaustively in terms of the optimization problem and sensitivity analysis. Section 3 then presented the numerical method utilized in the CFD solver, especially introducing the computational grid. The developed optimization solver was validated against the prototype in section 4, taking the well-known KJ66 turbine as test cases. At last, all the conclusions obtained in this manuscript were summarized in section 5.

## 2. OPTIMIZATION DETAILS

In this section, the design parameters and objective functions were introduced. Furthermore, the optimization algorithm and surrogate method were described.

### 2.1 Optimization Problem

In order to improve the single-stage turbine performance through optimization, without decreasing the mass flow rate. This was achieved through the optimization of the blade profile. Similar investigations were reported in literatures (Chen 2007; Huang 2019; Ennil *et al.* 2018; Zhou *et al.* 2018). Eq. (1) delineates the clear mathematic

formulation for the optimization (Arora, 2004; Mska *et al.* 2021). The objective was to obtain a new design with the maximum pressure ratio  $\pi$  and efficiency  $\eta$  in Eq. (2). The design variable vector  $\mathbf{x}$  includes the root middle curve ( $s_{1p_i}, i=1,2,3,4$ ) and tip middle curve ( $s_{2p_j}, j=1,2,3,4$ ) of the turbine guide vane, as well as the middle curve of the rotor blade root and tip ( $r_{1p_k}, k=1,2,3,4$  and  $r_{2p_n}, n=1,2,3,4$ , respectively). In order to meet the descending speed of the weight of all input data, the design variables were normalized using the  $z$ -score method, and the corresponding normalized parameters were represented by points on the original parameters, such as  $s_{1p_i}$ . The parameter  $m_{ori}$  refers to the mass flow rate that corresponds to the original blade profile in optimized working conditions.

$$\begin{cases} \max(\eta, \pi) \\ \mathbf{x} = \left( s_{1p_i}, s_{2p_j}, r_{1p_k}, r_{2p_n} \right) \\ s.t. m \geq m_{ori} \\ i, j, k, n \in \{1, 2, 3, 4\} \\ x \in (x_{min}, x_{max}) \end{cases} \quad (1)$$

$$\begin{cases} \pi = p_3^* / p_4^* \\ \eta = \left( 1 - T_4^* / T_3^* \right) / \left( 1 - (1/\pi)^{(\gamma-1)/\gamma} \right) \end{cases} \quad (2)$$

The elementary stage was generated through the superposition of the middle curve and thickness distribution. The structural angle distribution of the elementary stage of the blade was fitted by the Bezier curve, and the number of Bezier control points was four. The thickness distribution curve on the middle curve was fitted by the cubic spline, and the number of nodes of cubic spline was 50. Figure 2 presents the diagram for the blade parameterization. The blade stacking point was selected as the leading edge for the inlet guide vane, while centroid stacking was chosen for the rotor.

The global optimization was realized using a well-known approach, namely, the real-coded non-dominated sorting genetic algorithm-II (NSGA-II) (Davis, 1991; Deb *et al.* 2000). The process chart for NSGA-II is presented in Fig.3. The algorithm started with the initial population P. The optimized Latin hypercube sampling method was then executed for design samplings to speed up the optimization process (Mckay *et al.* 2000; Park 1994; Picus 1983). NSGA-II approaches were used to create the new Q individuals by selection, crossover and mutation at each generation. To this end, the new population  $P(t+1)$  was selected as the next population. These procedures were repeated until the convergence conditions of the NSGA-II were satisfied. The details of the algorithm, which were comprehensively described in the literature, (Davis 1991; Deb *et al.* 2000; Horn 1994), were not presented in the present study for the sake of brevity.

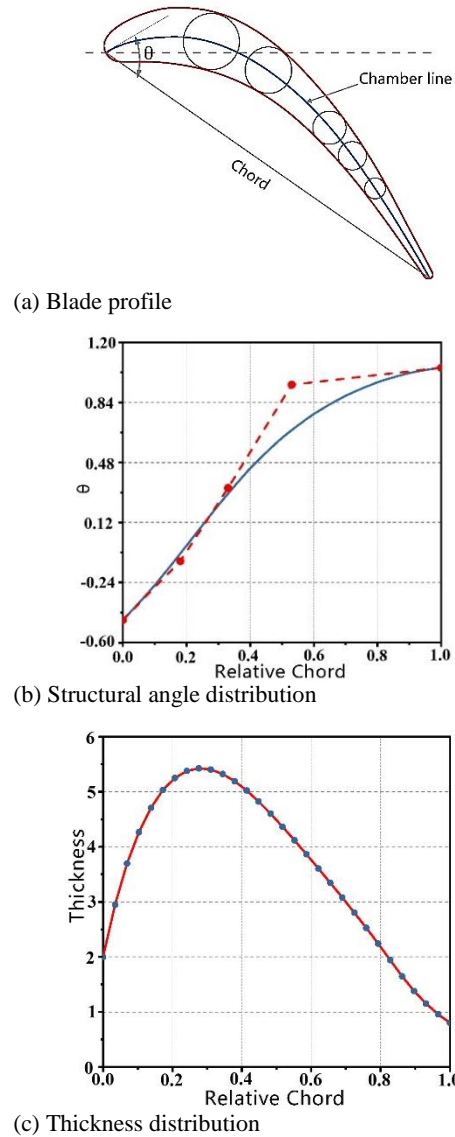


Fig. 2. Diagram for blade parameterization.

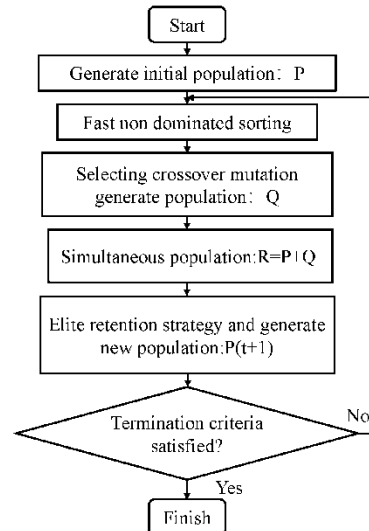


Fig. 3. Process chart for NSGA-II.

Solution for the optimization problem in Eq. (1) was realized using an artificial neural network optimization scheme in ANSYS WORKBENCH, and the whole flow chart is also given in Fig. 4. The present algorithm code was programmed with Python. The optimized Latin hypercube sampling method (Mckay *et al.* 2000; Park 1994; Picus 1983) was executed for the design samplings for the artificial neural network optimization scheme. Using these numerical solutions, the support vector regression (SVR) model (Vapnik *et al.* 2008; Müller *et al.* 1997) was applied to fit the objective-function values, which is less dependent on the number of samples, and is more suitable for regression analysis with small samples. Information drawn from neural network evaluation was finally utilized by a multi-objective genetic algorithm solver. Then, the optimization was validated against CFD solver of optimal solution. This process was repeated until the convergence of the optimization process was achieved.

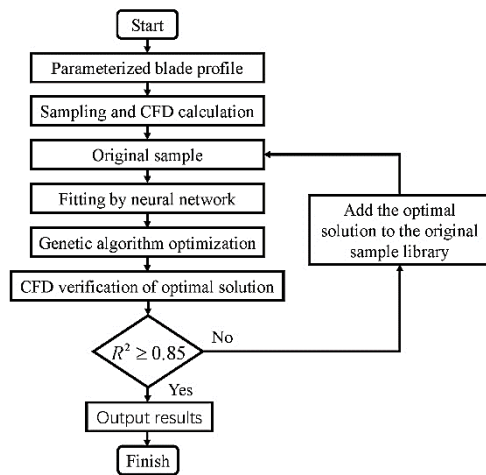


Fig. 4. The optimization flowchart.

## 2.2 Sensitivity Analysis

After the establishment of SVR model, Sobol sensitivity analysis method (Sobol, 2001; Sudret, 2008) is used to quantitatively study the influence of various optimization variables on adiabatic efficiency, flow rate and pressure ratio. The results revealed that the higher the sensitivity, the more sensitive the output variable is to the change of the input variable in the current value range. Sobol' method, which is a global analysis method to calculate the sensitivity of nonlinear response based on variance, can provide accurate information. Each  $S_{i_1, i_2, \dots, i_s}$  represents a sensitivity that determines the contribution of optimization parameters  $i_1, i_2, \dots, i_s$  on objectives. It can be defined as :

$$S_{i_1, i_2, \dots, i_s} = \frac{1}{\sigma^2} \left( \sum_{\alpha \in \{i_1, \dots, i_s\}} u_\alpha^2 \langle \Psi_\alpha \Psi_\alpha \rangle \right) \quad (3)$$

The total sensitivity methods can be derived as (Sudret 2008; Sobol 1990):

$$S_{j_1, j_2, \dots, j_s}^T = \sum_{(i_1, i_2, \dots, i_s) \in \emptyset_{i_1, \dots, i_s}} S_{i_1, \dots, i_s} \quad (4)$$

## 3. NUMERICAL ANALYSIS

### 3.1 Flow Solution

In this flow solution, the Navier-Stokes equations are solved by a numerical procedure based on upwind finite-volume solver, ANSYS CFX 2019 R3. The total pressure and total temperature at the inlet were set to 192 000.0 Pa and 973.0 K, respectively. The working fluid, air, was considered as the ideal gas. Solutions were obtained by outlet static pressure until the steady state is reached. The inflow vector was set to be axial to the rotational axis. The solid surfaces were considered to be smooth with no-slip and adiabatic conditions. The  $k-\omega$  turbulence model was applied to close the equation set. The physical time scale was set to  $8 \times 10^{-5}$  seconds. These running conditions are tabulated in Table 1.

Table 1 Numerical solution conditions

Parameters	Value
Total temperature (K)	973
Total pressure (Pa)	192 000
Circumferential flow angle (°)	0
Radial flow angle (°)	0
Turbulence model	$k-\omega$
Static pressure on design point (Pa)	110 000

For the calculation convergence, the converged solutions for the original stage are illustrated in Fig. 5. It can be observed that the simulation processes converge after 300 steps. Furthermore, the pressure ratio and efficiency at the designed mass flowrate of 0.22 kg/s was 1.4956 and 83.717%, respectively.

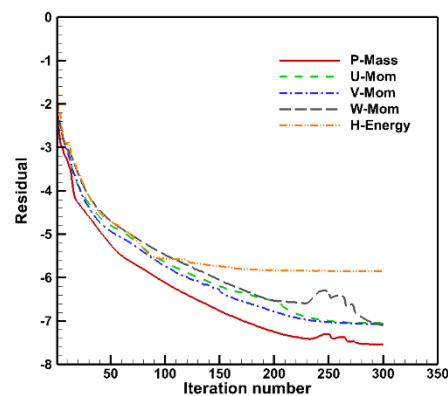


Fig. 5. Convergence history.

### 3.2 Computational Grid

For the mesh generation, the domain was decomposed into two parts, namely, the guide vane and rotor, and each mesh was separately generated. Merely one passage of each of the turbine guide vanes and rotor sections was meshed for flow

solution. The two domains were connected using the mixing-plane method. Then, a rotational periodic boundary condition was applied, and the tip clearance was modelled as 0.1 mm at the rotor domain.

Meshes for the guide vane domain and rotor domain were generated independently. The results for the efficiency and total pressure ratio are presented in Fig.6. The grid-independency test was performed with a change in grid size from 0.2 million to 1.6 million. The values for the efficiency and pressure ratio dot changed with the grid size exceeds 1 200 000. Therefore, 0.6 million grid points were applied for the guide vane, and 0.7 million grid points were applied for the turbine rotor. The computational domain is presented in Fig.7. The mesh generation method was based on a boundary layer with 1e-4 m layer thickness.

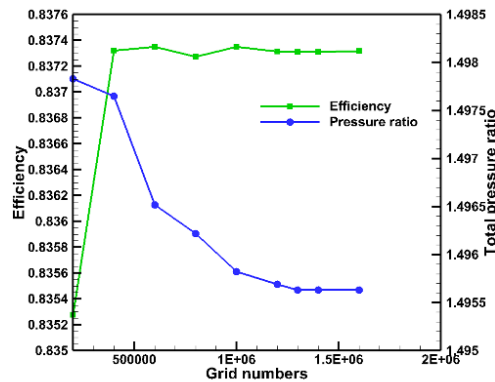
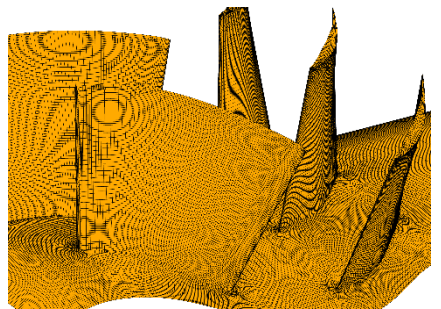


Fig. 6. Grid-independency test result.



(a) 3D Mesh



(b) B2B Mesh

Fig. 7. Computational grids.

#### 4. APPLICATIONS

In this section, KJ66 turbine was presented as the validation for the developed optimization method with respect to the off-design performances and the flow details.

##### 4.1 Accuracy of SVR Model and Sensitivity Analysis

Since the SVR model significantly affects the optimization precision, the quality was validated before the optimization (Vapnik *et al.* 2008; Müller *et al.* 1997). In the validation procedure, the cases in the training and testing databases were randomly generated. The results in the testing database are presented in Fig.8. Next, the accuracy was compared with the CFD simulation. The comparison results are presented in Fig.8. Based on the former theory, the LIBSVM toolbox (Ferrari, 2008) was used to fit the SVR data. The coefficient of determination  $R^2$  was used to evaluate the model (Zhao and Wen, 2003):

$$SST = \sum_i (y_i - \bar{y})^2$$

$$SSR = \sum_i (y_i - f_i)^2 \quad (5)$$

$$R^2 = 1 - \frac{SSR}{SST}$$

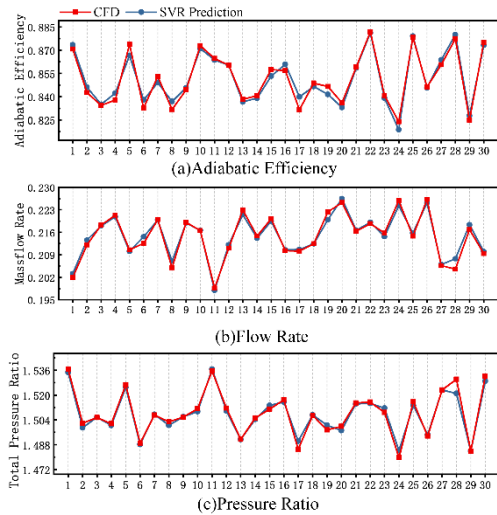
Where:  $\bar{y}$  refers to the mean value of the testing databases:

$$\bar{y} = \frac{1}{n} \sum_{i=1}^n y_i \quad (6)$$

Where:  $y_i$  refers to the real value of the testing databases, and  $f_i$  refers to the predicted value of the surrogate model of the testing databases. SST refers to the sum of the variance. The larger the SST value, the more discrete the data became. When the accuracy of the surrogate model was high, SSR became close to 0 and  $R^2$  became close to 1. Therefore, the larger the  $R^2$  value, the better the fitting effect of the surrogate model.

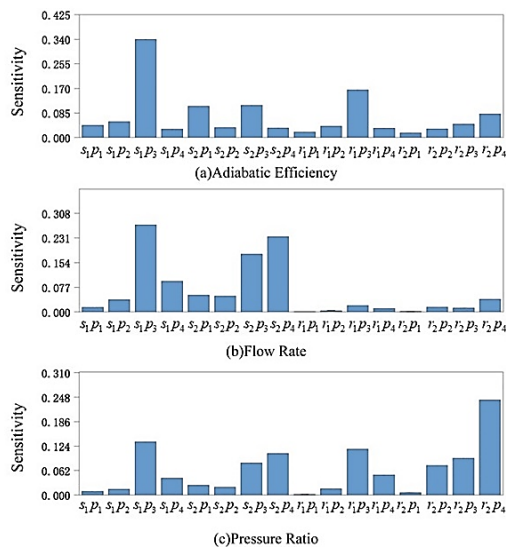
The results in Fig.8 present the adiabatic efficiency, flow rate and pressure ratio between the CFD calculation and prediction through the SVR for 30 different testing databases. The comparisons for the CFD simulation and SVR prediction on these performances were presented in different colors. The coefficient  $R^2$  for adiabatic efficiency, flow rate and pressure ratio was 0.96397, 0.97250 and 0.97350, respectively. There were no significant differences between the CFD calculation and SVR prediction. The comparisons in Figure 8 present the excellent consistency between the SVR predictions and the CFD calculate data.

Figure 9 presents the Pareto-sensitivity of the design variables determined using the Sobol sensitivity analysis method (Sobol, 2001). As visible, two



**Fig. 8. Performance of SVR on testing databases.**

design variables,  $s_1p_3$  and  $r_1p_3$ , had a significant influence on the adiabatic efficiency, while the other design variables were not significantly sensitive to this. The reason for this was because severe flow separation occurs at the stator and rotor blade root, and the changes in these two parameters effectively increases or decreases the separation zone. As shown in Fig.9(b), the flow rate at the turbine stage was mainly affected by the guide vane, and the influence of the rotor part on the flow rate was almost ignored, because the blockage initially occurs in the stator. Furthermore, the design variable  $r_2p_4$  was the most sensitive to the objective function pressure ratio. For the turbine rotor, a secondary leakage flow occurred at the rotor tip, causing the pressure ratio to be more sensitive to the geometry.



**Fig. 9. Sensitivity analysis.**

**4.2 Results**

The running conditions for the turbine are presented in Table 1. Typically, 500 generations, containing 1000 individuals, were used in NSGA-II. The

crossover and mutation probabilities were set to 0.9 and 0.05, respectively.

In order to determine the optimization convergence, two indexes were introduced, namely, hypervolume (HV) and spacing metric (SP). The details of these indexes, which are comprehensively described in the literature (Zitzler *et al.* 1999; Schott 1995), were not presented in the present study. The optimization convergences are presented in Fig.10. As shown in the figure, the optimization process converged after 500 generations.

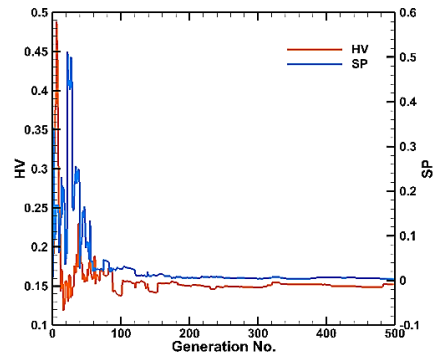


**Fig. 10. Convergence of the selected optimum point.**

The trade-off diagram between the two design objectives, which are the efficiency and total pressure ratio, is presented in Fig.11, illustrating the feasible and infeasible solutions. As visible, the shape of the Pareto optimum fronts resembled a convex curve. Comparing with the performance before optimization, the two points with the worst performance of a single objective in the Pareto frontier solution (the leftmost and bottom two points in the figure) have far exceeded the efficiency and pressure ratio of the prototype. In the present study, the performance of the Pareto fronts far exceeded the efficiency and pressure ratio of the prototype, fully showing that the optimization was effective.

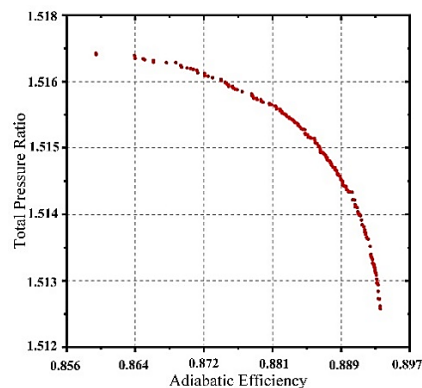
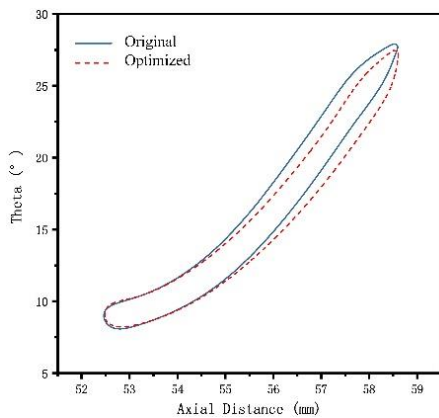


**Fig. 11. Trade-off chart for the optimization.**

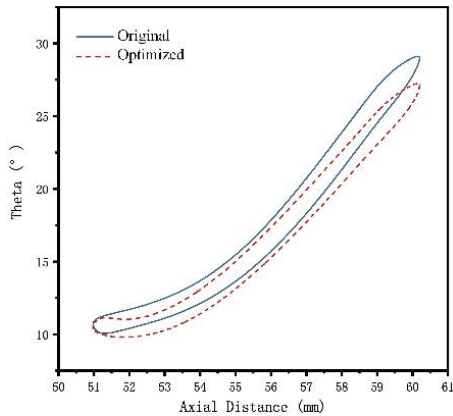
From the 1000 optimization samples, the design candidate was selected according to the weight of adiabatic efficiency, the total pressure ratio of 3:1, and the objective date, as shown in Table 2.

**Table 2 Design parameters for the design candidate**

Variable	Value	Variable	Value
$s_1p_1$	0.000136	$s_1p_2$	1.595711
$s_1p_3$	3.878202	$s_1p_4$	7.2075237
$s_2p_1$	-1.19990	$s_2p_2$	2.112996
$s_2p_3$	6.178424	$s_2p_4$	9.503913
$r_1p_1$	-0.062714	$r_1p_2$	-1.187698
$r_1p_3$	-1.998378	$r_1p_4$	-4.415964
$r_2p_1$	-0.090624	$r_2p_2$	-1.368491
$r_2p_3$	-3.166189	$r_2p_4$	-6.237549



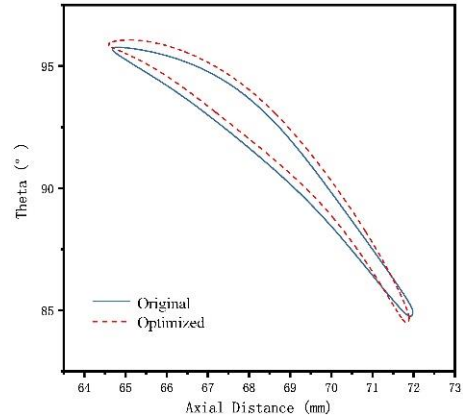
(a) Guide vane root



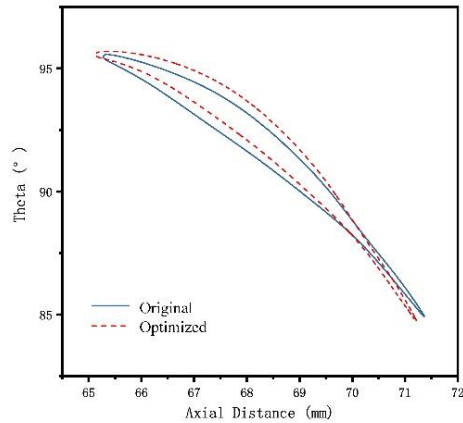
(b) Guide vane top

**Fig. 12. Geometry comparison for the guide vane.**

In order to distinguish the change of blade geometry more clearly, the geometric comparison of blade at the root and top before and after optimization are presented in Fig. 12 and 13. As shown in the figures, the part of the guide blade root near the trailing edge considerably changed, the curvature of the optimized blade profile was significantly reduced, and there was no significant difference at the leading edge. Located at the tip, the leading edge structural angle of the blade



(a) Rotor root



(b) Rotor top

**Fig. 13. Geometry comparison for the rotor.**

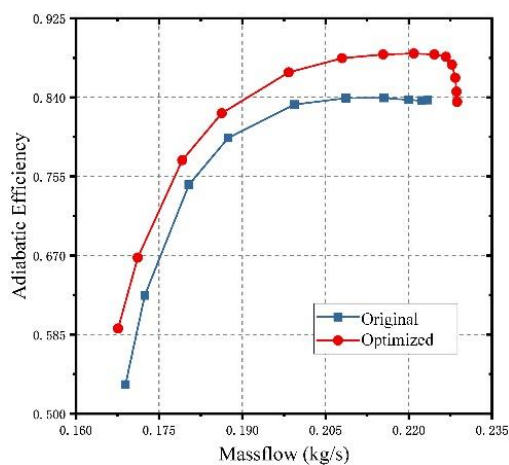
obviously increased, which led to the increase in curvature of the blade at the leading edge, and the geometry transition of the tip trailing edge was smoother. It is noteworthy that flow separation tended to occur near the trailing edge. Hence, a gentle profile transition was beneficial in reducing the flow separation at the trailing edge for the stator. In comparison, the lean angle of the optimized rotor increased at the blade root and tip, which was more conducive for the air to pass through the turbine blade, improving the pressure ratio of the turbine rotor. Combined with Fig. 9, the most influential geometric locations for adiabatic efficiency and pressure ratio were the trailing edge of the guide vane root, the leading edge and trailing edge of the guide vane tip, and the trailing edge portion of the rotor. Thus, it is through this corresponding position that the most obvious geometric changes took place.

The performances calculated by the CFD simulation at the design candidate and predicted by the SVR, along with the reference values, are presented in Table 3. As illustrated in the table, the optimized turbine had a significant gain in both objectives, the adiabatic efficiency of the main objective improved by approximately 5.95%, and the total pressure ratio increased by approximately 0.9%. Furthermore, the results are in good agreement, being an error of 0.08% for efficiency

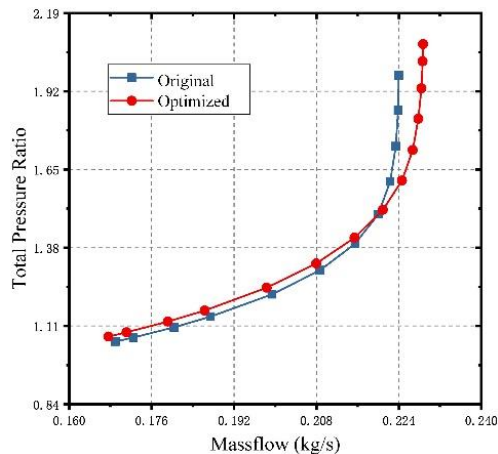
and 0.167% for pressure ratio. This shows the adequacy of the present optimization method on single-stage turbine optimization.

**Table 3 Optimization results for the KJ66 turbine**

Variable	Efficiency	PR	Mass
Original	0.837171	1.49562	0.2200130
SVR	0.88627	1.51308	0.2200130
CFD	0.887022	1.51056	0.220908
Error	0.08%	0.167%	0.4%
Increase	5.95%	0.9%	0.4%



(a) Efficiency



(b) Pressure ratio

**Fig. 14. Performance characteristics for the KJ66 turbine.**

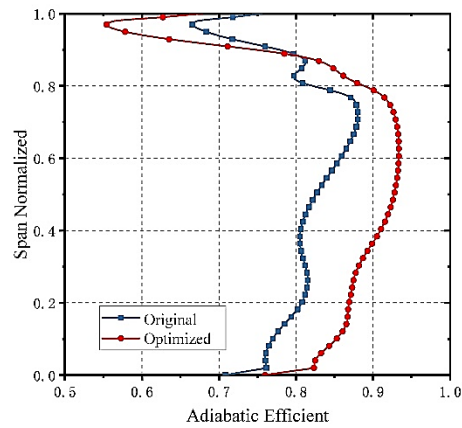
A further investigation of the off-design performance of the original and optimized KJ66 turbine has been implemented. The results are presented in Fig.14. The adiabatic efficiency of the original turbine tended to be constant when the flow rate decreased. However, the efficiency of the optimized turbine increased with the decrease in flow rate from the

blockage point. When the flow rate decreased to 0.205 kg/s, the efficiency of both the optimized and original turbines began to rapidly decrease. However, under the same flow rate, the efficiency of the optimized turbine remained higher than that of the prototype, exhibiting an excellent optimization effect. The near-choking flow rate for the optimum shape significantly increased, when compared to the prototype. The reason for this was because the throat area of the optimized stator increased, resulting in an enhanced flow capacity. As shown in Fig.14(b), when the flow rate was less than 0.22 kg/s, the pressure ratio in the optimized turbine was slightly higher than that in the prototype. With the increase in flow rate, the pressure ratio for the optimized blade became slightly lower than that for the original blade at the same flow rate. However, the maximum pressure ratio that the optimized turbine could achieve remained higher than that for the prototype. In general, the optimization effect of the pressure ratio was slightly weaker than that for efficiency, which was due to the priority of efficiency gain when selecting the design candidate from the Pareto fronts.

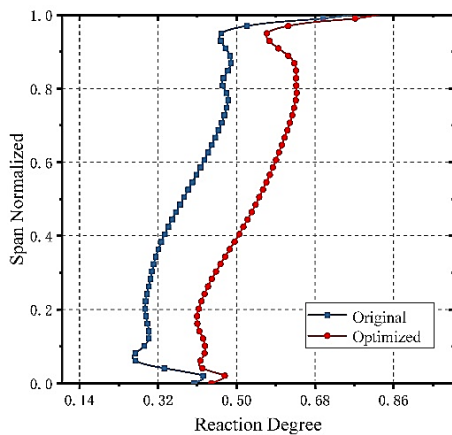
The flow pattern for the KJ66 turbine was further analyzed, and the results were compared (Fig. 15) in terms of the adiabatic efficiency and reaction force spanwise distribution at the turbine stage. The efficiency increased from 83.7% to 88.7%. As shown in Fig.15(a), after optimization, the efficiency at the 0%-90% spanwise positions significantly improved, while the efficiency at more than 90% of the blade tip position slightly decreased. The reaction force distribution form of the whole turbine stage, along the blade root to the blade tip, did not change, and this significantly improved, along with the whole blade. The total reaction force increased from 0.409 to 0.520 in the prototype, as shown in Fig. 15(b). As it is known, the reaction force is the ratio of the expansion work of the rotor to the actual work of the stage, that is,  $\Omega = (h_1 - h_2)/L_u$ , where  $h_1$ ,  $h_2$  and  $L_u$  refers to the inlet enthalpy, outlet enthalpy and actual work, respectively. The increase in reaction force means that the gas expansion process occurs more in the rotor. As a result, the gap leakage loss at the rotor tip was more serious, leading to the decrease in adiabatic efficiency at the blade tip. This is consistent with the results presented in Fig. 15(a).

The static pressure ratio in the stator and the total pressure ratio in the rotor were compared in detail, as shown in Fig. 16. The static pressure ratio in the guide vane decreased from 1.33 to 1.26, and the total pressure ratio in the rotor increased from 1.44 to 1.48. In terms of distribution, the static pressure ratio for the guide vane uniformly decreased along the whole blade. However, the pressure ratio for the rotor significantly increased, which is consistent with the conclusion presented in Fig. 15(b).

The Mach number distribution at the 10%, 50% and 90% spanwise positions of the turbine stage blades is presented in Fig. 17(a)-17(c). As shown in the figures, flow separation occurred at approximately the 50% chord of the suction surface of the original guide, and the separation area became obvious. After optimization, the leading edge angle of attack on the



(a) Efficiency distribution



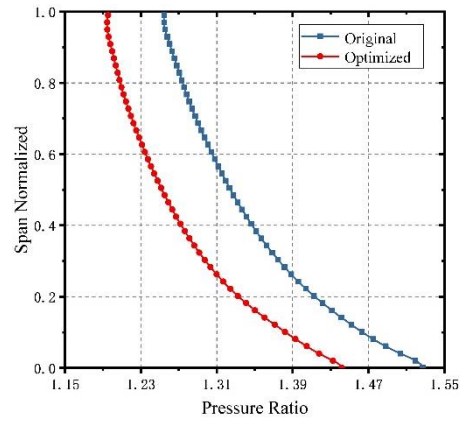
(b) Reaction force distribution

**Fig. 15. Adiabatic efficiency and reaction force spanwise distribution at the turbine stage.**

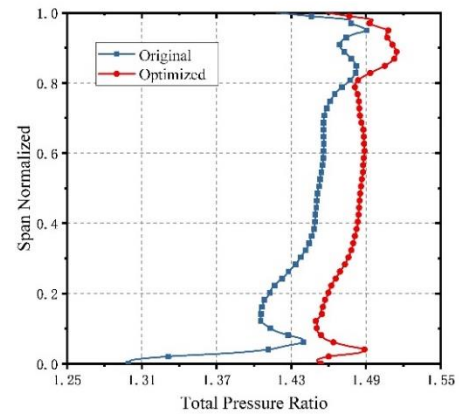
guide vane decreased, the separation position moved backward, the separation zone reduced, and the flow field in the guide vane improved. Furthermore, a boundary layer separation occurred at the trailing edge of the original rotor blade at the 50% spanwise position. Moreover, the flow in the optimized rotor blade significantly improved, as shown in Fig. 17(b).

Figure 18 presents the entropy distribution on the suction surface of the turbine guide vane on the design point. The optimized profile had lower entropic values than those for the prototype. Furthermore, the original profile had significantly higher entropic values in front of the suction due to the large flow loss at the leading edge, while the high entropy area at the leading edge of the optimized blade profile almost disappeared, indicating that the flow loss at the leading edge was reduced.

The streamline diagram for the guide vane is presented in Fig.19. As shown in the figure, there is a clear separation zone at the front of the prototype, which may be due to the large angle of attack at the inlet. The optimization increased the leading edge angle, improved the distribution of the inlet angle of attack, and effectively suppressed the flow

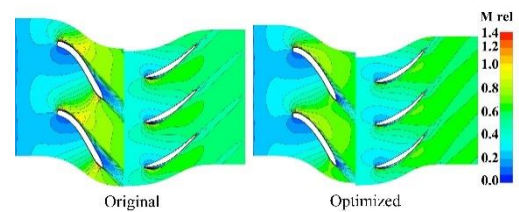


(a)

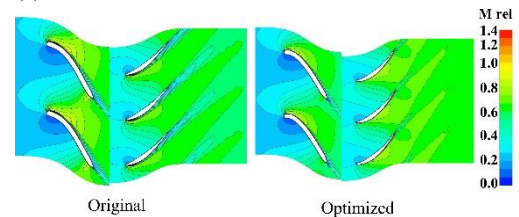


(b)

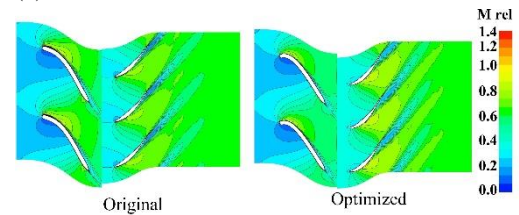
**Fig. 16. Spanwise distribution of the guide static pressure ratio and rotor total pressure ratio.**



(a) 10%



(b) 50%



(c) 90%

**Fig. 17. Mach number distribution at the 10%, 50% and 90% spanwise position near the peak efficiency point.**

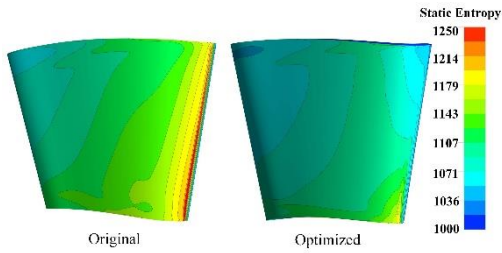


**Fig. 18. Entropy distribution on the suction surface of the turbine guide vane.**

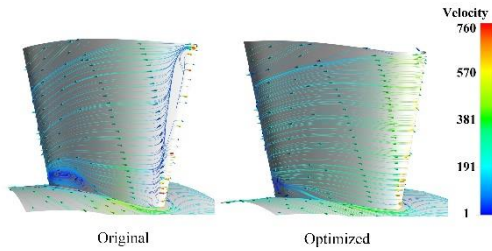
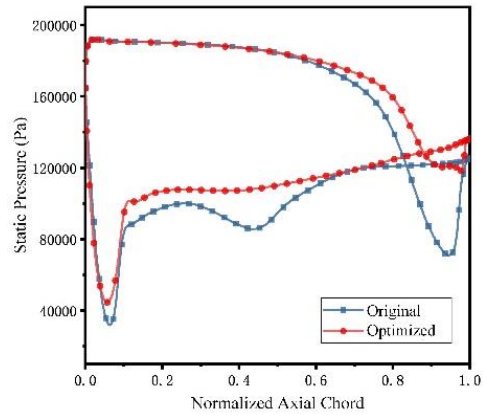


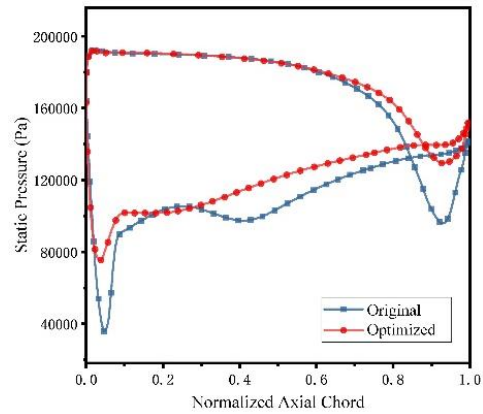
**Fig. 19. Streamline diagram for the turbine guide vane.**

In order to more clearly and quantitatively observe the change in flow parameters, the static pressure spanwise distribution at 10%, 50% and 90% on the guide vane was summarized, as shown in Fig.20. Overall, the static pressure of the pressure surface at the first 60% chord was constant, while the static pressure at the last 40% chord increased, when compared to those obtained from the original stage. Furthermore, there were obvious pressure mutations at the suction leading edge of the three spanwise positions of the prototype, and this was due to the flow separation at the pressure leading edge of the guide (Fig.18). However, the pressure distribution at the leading edge of the optimized blade was smoother (especially at the 50% and 90% spanwise positions). In addition, the pressure gradient of the new design blade significantly decreased, which was beneficial to restrain the boundary layer separation.

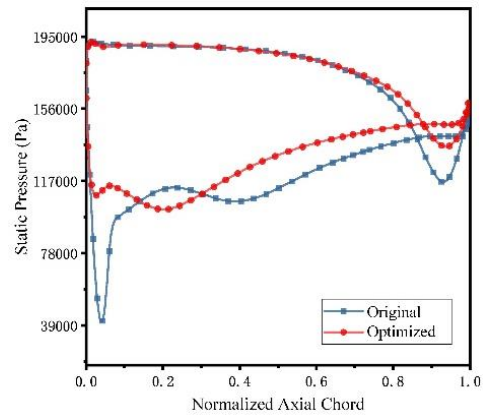
The entropy distribution for the suction surface of the rotor is presented in Fig.21. As visible, the entropy at the leading edge of the prototype was large, indicating that the flow loss at the leading edge was large. After optimization, the entropy at the leading edge decreased, especially at the leading edge tip, indicating that the flow at the leading edge significantly improved. This was also confirmed in the streamline diagram for the turbine rotor, as presented in Fig.22. The flow separation at the leading edge of the original rotor started approximately from the 10% chord of the root suction surface, and this extended approximately to the 80% spanwise position of the blade leading edge. However, the separation area at the optimized passage significantly decreased, and merely the flow separation existed below the 30% spanwise position. The change in blade leading edge flow state shows that the inlet structure angle of the original turbine rotor could not match the outlet flow angle of the guide vane well, leading to the unreasonable distribution of rotor leading attack angle.



(a) 10%



(b) 50%



(c) 90%

**Fig. 20. Static pressure distribution on the guide vane surface.**

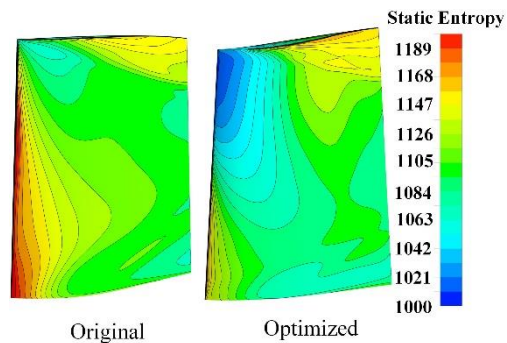


**Fig. 21. Entropy distribution on the suction surface of the rotor.**

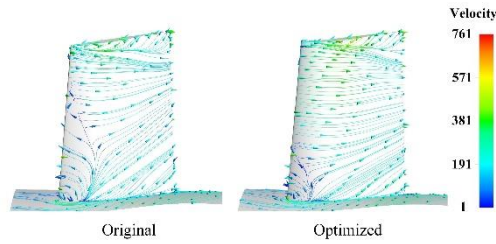


**Fig. 22.** The streamline diagram for the rotor.

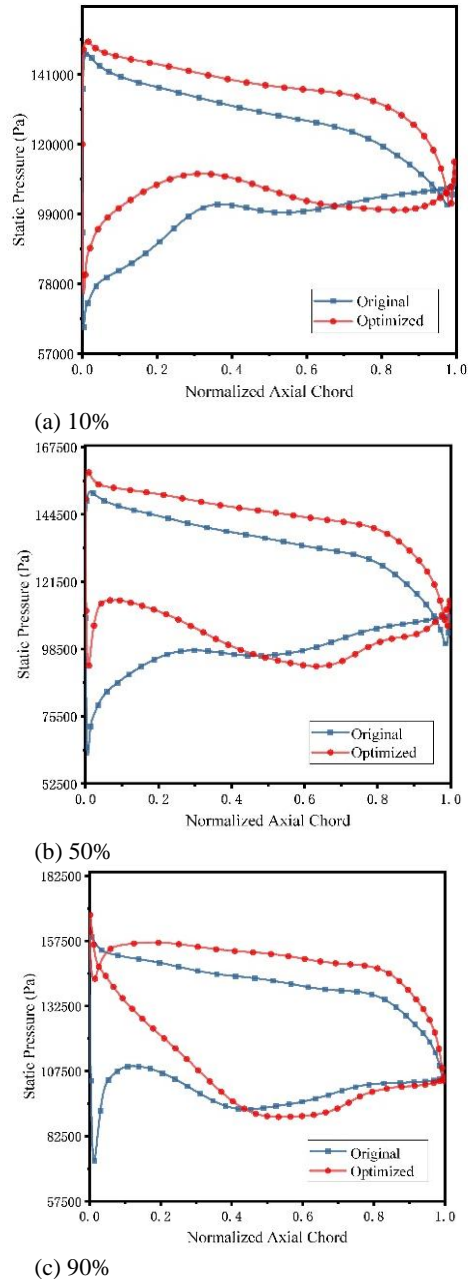


**Fig. 23.** Static pressure distribution on the rotor surface.

Figure 23 illustrates the static pressure spanwise distribution at 10%, 50% and 90% of the rotor. The optimum shape of the rotor had the highest pressure along the whole blade. It was considered that the increase in lean angle significantly enhanced the expansion ability of the gas. The static pressure at the

suction surface at three spanwise significantly increased before approximately 70%, 50% and 40% chord, respectively, but this decreased at the other positions. Furthermore, the load distribution of the blade at the 50% spanwise position changed from the original "C" loaded to post-loaded. The leading load of the optimized blade obviously decreased, and the angle of attack became smaller than that of the prototype, effectively weakening the flow separation of the rotor. Hence, the joint optimization of the guide vane and rotor made the aerodynamic matching effect better.

## 5. CONCLUSION

In the present study, the optimization of a small single-stage turbine was presented and discussed. The optimization was performed by designing the middle curve using NSGA-II to maximize the efficiency and total pressure ratio of the turbine stage. The results have been compared with the prototype. The main conclusions are summarized below:

- (1) Under the design condition, flow separation occurred on the pressure surface of the guide vane, resulting in a sharp rise in flow loss. The optimized profile was mainly characterized by the increase in leading edge, while the distribution of the inlet angle of attack improved. The gentle distribution of inlet angle of attack can effectively suppress the flow separation, thereby reducing the loss.
- (2) Compared to the original profile, the lean angle of the rotor increased, which was more conducive for the air flowing through the turbine blade, improving the pressure ratio of the turbine rotor. However, the gap leakage loss at the rotor tip became more severe, causing the adiabatic efficiency to decrease.
- (3) These optimal solutions show that the adiabatic efficiency increased by 5.95%, and that the pressure ratio improved by 0.9%, when compared to the prototype. The developed optimization method provides an accurate and efficient tool for the small gas turbine optimization.

## REFERENCES

- Ainley, D. and G. Mathieson (1951). An examination of the flow and pressure losses in blade rows of axial-flow turbines. *Technical report 1-35*, HMSO.
- Arora, J. (2004). *Introduction to optimum design* (Elsevier).
- Balje, O. (1968). Axial turbine performance evaluation. Part A—Loss-Geometry relationships. *Journal of Engineering for Gas Turbines and Power* 90, 341–348.
- Basson, J. (2014). *Design methodology of an axial-flow turbine for a micro jet engine*. Ph. D. thesis, University of Stellenbosch, South Africa.

- Benner, M. W., S. A. Sjolander and S. H. Moustapha (2006a). An empirical prediction method for secondary losses in turbines-part I: A new loss breakdown scheme and penetration depth correlation. *Journal of Turbomachinery* 128(2), 273-280.
- Benner, M. W., S. A. Sjolander and S. H. Moustapha (2006b). An empirical prediction method for secondary losses in turbines-part II: A new secondary loss correlation. *Journal of Turbomachinery* 128(2), 281-291.
- Benner, M. W., S. A. Sjolander and S. H. Moustapha (2004). Measurements of secondary flows downstream of a turbine cascade at off-design incidence. In *Proceeding of ASME TURBO EXPO 2004*, Vienna, Austria, GT2004-53786.
- Chen, L. H. (2007). *Aerodynamic optimization design of compressor blade based on neural network and genetic algorithm*. Ph. D. thesis, Northwestern Polytechnical University, Xi an, China.
- Craig, H. and H. Cox (1970). Performance estimation of axial flow turbines. *Proceedings of the Institution of Mechanical Engineers* 185, 407-424.
- Davis, L. (1991). *Handbook of genetic algorithms. Handbook of Genetic Algorithms*.
- Deb, K., S. Agrawal, A. Pratap and T. Meyarivan (2000). A Fast Elitist Non-dominated Sorting Genetic Algorithm for Multi-objective Optimization: NSGA-II. *Lecture Notes in Computer Science* 1917, 849-858.
- Dunham, J. and P. M. Came (1970). Improvements to the ainley-mathieson method of turbine performance prediction. *Journal of Engineering for Gas Turbines and Power* 92, 252-256.
- Ennil, A., R. K. Al-Dadaha, S. Mahmouda and A. M. Al-Jubori (2018, January). Optimization of small scale axial air turbine using ansys cfx. In *Proceedings of 22 nd the IIER international conference*, London, United Kingdom.
- Ferrari, V. (2008). Libsvm: A library for support vector machines. *ACM Transactions on Intelligent Systems and Technology*.
- Horn, J. (1994, July). A niched Pareto genetic algorithm for multiobjective optimization. In *Proceedings of the first IEEE conference on evolutionary computation*, IEEE.
- Huang, M. X. (2019). *Research on Blade Optimization Design of Analysis Code Using Artificial Neural Network and Genetic Algorithm*. Master's thesis, Nanjing University of Aeronautics and Astronautics, Nanjing, China.
- Kacker, S. C. and U. Okapuu (1982). A mean line prediction method for axial flow turbine efficiency. *Journal of Engineering for Power* 104,1 (1).
- Li, T. Y. (2019). *Three-dimensional Numerical Simulation of An Entire Micro Turbojet Engine*. Ph. D. thesis, Dalian University of Technology, China.
- Massardo, A., A. Satta and M. Ma (1990). e axial flow compressor design optimization. part ii: through-flow analysis. *Journal of Turbomachinery* 112(3), 405-410.
- Mckay, Beckman and Conover (2000). A comparison of three methods for selecting values of input variables in the analysis of output from a computer code. *Technometrics* 42(1), 55-61.
- Mohamed, M. H. and S. Shaaban (2013). Optimization of blade pitch angle of an axial turbine used for wave energy conversion. *Energy* 56, 229-239.
- Moroz, L., Y. Govoruschenko, L. Romanenko and P. Pagur (2004, June). Methods and tools for multidisciplinary optimization of axial turbine stages with relatively long blades. In *Asme turbo expo: Power for land, sea, and air*, Vienna, Austria, GT2004-53379.
- Moustapha, H., A. Cooling, M. F. Zelesky and D. Japikse (2003). Axial and radial turbines. *Concepts NREC*.
- Moustapha, S. H., S. C. Kacker and B. Tremblay (1990). An improved incidence losses prediction method for turbine airfoils. *Journal of Turbomachinery* 112, 267-276.
- Mohamad, S. K., R. Mehrdad, S. Saeed, H. Patrick and N. Ahmad (2021). Robust optimization of the NASA C3X gas turbine vane under uncertain operational conditions. *International Journal of Heat and Mass Transfer* 164.
- Müller, K. R., A.J. Smola, G. Ratsch, B. Schlkopf, J. Kohlmorgen and V. Vapnik (1997, October). Predicting time series with support vector machines. In *ICANN '97: Proceedings of the 7th international conference on artificial neural networks*, Springer, Berlin, Heidelberg.
- Murray, P. W. (2009). *Microturbine for micro-cogeneration application*. Ph. D. thesis, Queen's University, Canada.
- Park, J. S. (1994). Optimal Latin-hypercube designs for computer experiments. *Journal of Statistical Planning & Inference* 39, 95-111.
- Picus, D. (1983). Computed tomography in the staging of esophageal carcinoma. *Radiology* 146, 433-438.
- Tian, B. L. (2003). A Survey of the Development of Engines for the Unmanned Aircraft and the Cruise Missile in the World. *Aeroengine* 29(4), 51-54.
- Schott, J. R. (1995). *Fault tolerant design using single and multicriteria genetic algorithm optimization*. Ph. D. thesis, Cambridge, England.

- Smith, S. F. (1965). A simple correlation of turbine efficiency. *Aeronautical Journal* 69, 467–470.
- Sobol, I. (1990). On sensitivity estimation for nonlinear mathematical models. *Keldysh Applied Mathematics Institute*: 112–118.
- Sobol, I. M. (2001). Global sensitivity indices for nonlinear mathematical models and their Monte Carlo estimates. *Mathematics and Computers in Simulation* 55, 271–280.
- Sudret, B. (2008). Global sensitivity analysis using polynomial chaos expansions. *Reliability Engineering & System Safety* 93, 964–979.
- Vapnik, V., S. E. Golowich and A. Smola (2008). Support vector method for function approximation, regression estimation, and signal processing. *Advances in Neural Information Processing Systems* 9, 281–287.
- Wakeley, J. and J. Hey (1997). Estimating ancestral population parameters. *Genetics* 145, 847–855.
- Yang, W. and R. Xiao (2014). Multiobjective optimization design of a Pump–Turbine impeller based on an inverse design using a combination optimization strategy. *Journal of Fluids Engineering* 136, 249–256.
- Zhao, W. and X. N. Wen (2003). *Applied Statistics Course*. Xidian University, Xian, China.
- Zhou, L., F. Xiang and Z. Wang (2018). CFD investigation on the application of optimum non-axisymmetric endwall profiling for a vaned diffuse. *Journal of Applied Fluid Mechanics* 11, 1703–1715.
- Zhu, J. and S. A. Sjolander (2005, June). Improved profile loss and deviation correlations for axial-turbine blade rows. In *Asme turbo expo: Power for land, sea, and air*, Reno-Tahoe, Nevada, USA, GT2005-69077.
- Zitzler, E., K. Deb and L. Thiele (1999). Comparison of multiobjective evolutionary algorithms on test functions of different difficulty.